

Supplementary Information

DNA translocation through an array of kinked nanopores

*Zhu Chen¹, Yingbing Jiang², Darren R. Dunphy¹, David P. Adams², Carter Hodges²,
Nanguo Liu¹, Nan Zhang³, George Xomeritakis¹, Xiaozhong Jin⁴, N.R. Aluru⁴, Steven J.
Gaik⁵, Hugh W. Hillhouse⁵, and C. Jeffrey Brinker^{1,2,6}*

1. Department of Chemical & Nuclear Engineering and Center for Micro-Engineered Materials, The University of New Mexico; 2. Sandia National Laboratories; 3. School of Pharmacy, The University of New Mexico; 4. Department of Mechanical Science and Engineering and Beckman Institute for Advanced Science and Technology, the University of Illinois at Urbana-Champaign; 5. School of Chemical Engineering, Purdue University; 6. Department of Molecular Genetics and Microbiology, the University of New Mexico

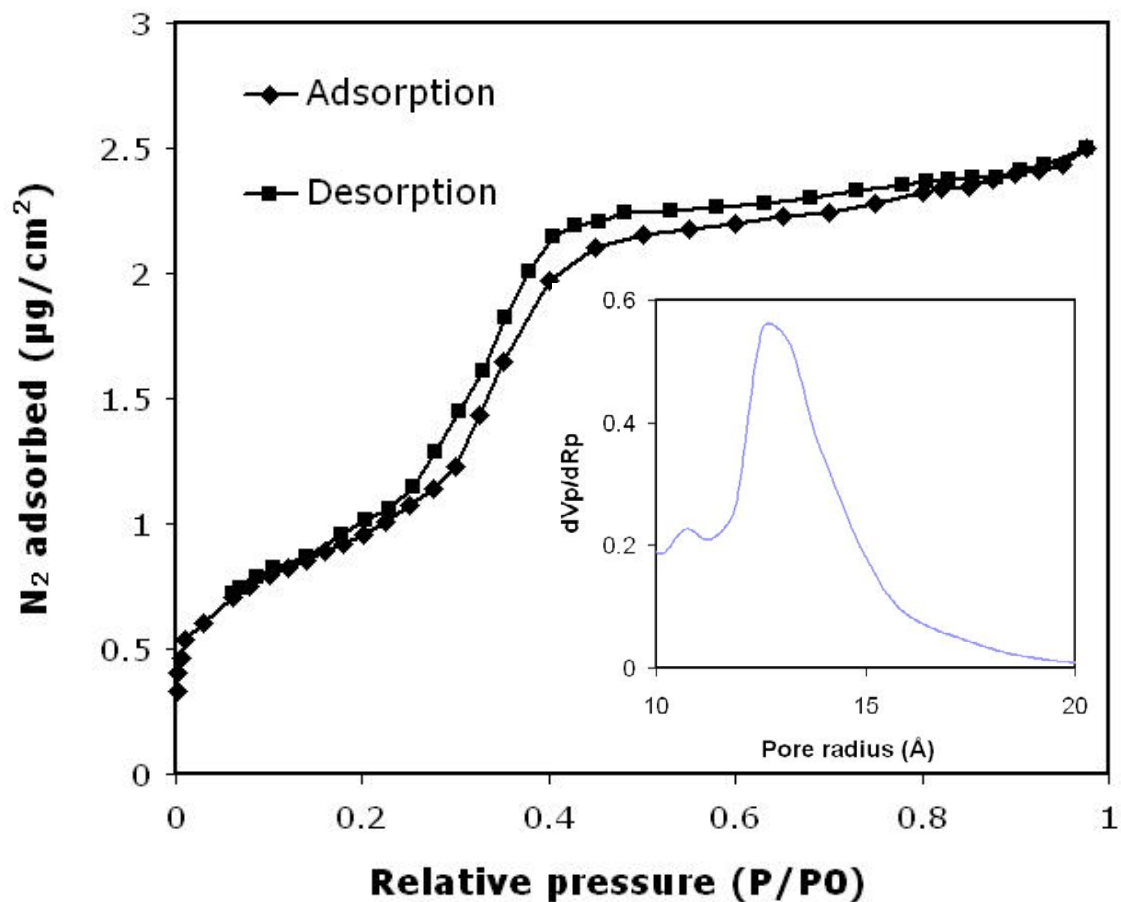


Figure S1. Nitrogen sorption isotherm acquired for thin film mesophase using SAW technique and pore size distribution calculated by the BJH method based on the adsorption branch of the isotherm.

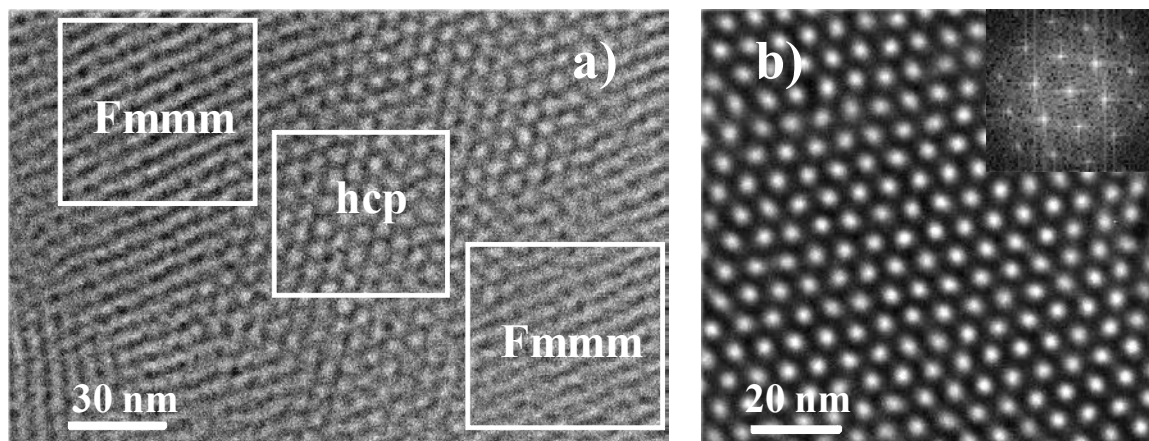


Figure S2. TEM plan view showing a) coexistence of distorted bcc mesophases ($Fmmm$) and hcp mesophases and b) a (001) orientated hcp region (with FFT inset). The image in Figure S2 (b) was obtained under overfocus conditions (+1800 nm) with accelerating voltage of 200 kV, yielding reversed contrast relative to the honeycomb pattern generally observed for $P6_3/mmc$ along $[001]$ ¹, with bright spots here corresponding to silica walls and dark areas arising from empty pores.

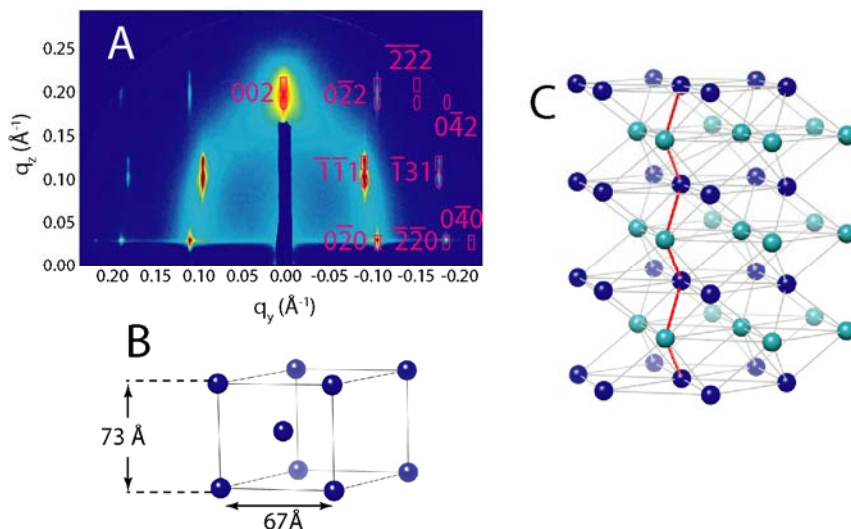


Figure S3. A) Typical GISAXS data for a self-assembled porous silica film (ca. 300 nm thick), showing the presence of a highly-oriented predominantly *Fmmm* phase (distorted bcc) along with a diffuse scattering ring arising from domains that are not highly oriented with respect to the plane of the substrate or from regions with globular micellar packings with structural order intermediate to distorted bcc and hcp structures. Ovals and rectangles signify the predicted positions of diffraction from the incident and reflected beam, respectively. B) Unit cell dimensions for the hcp phase fit to the GISAXS data in Figure 2A of main text (not the GISAXS data in Figure S3). C) Schematic of the [001]-oriented hcp phase, showing lattice points (here representing the positions of pores) in alternate (001) planes signified by color and the 12-fold coordination characteristic of hcp packing indicated by grey lines. A direct pathway through the lattice is labeled in red.

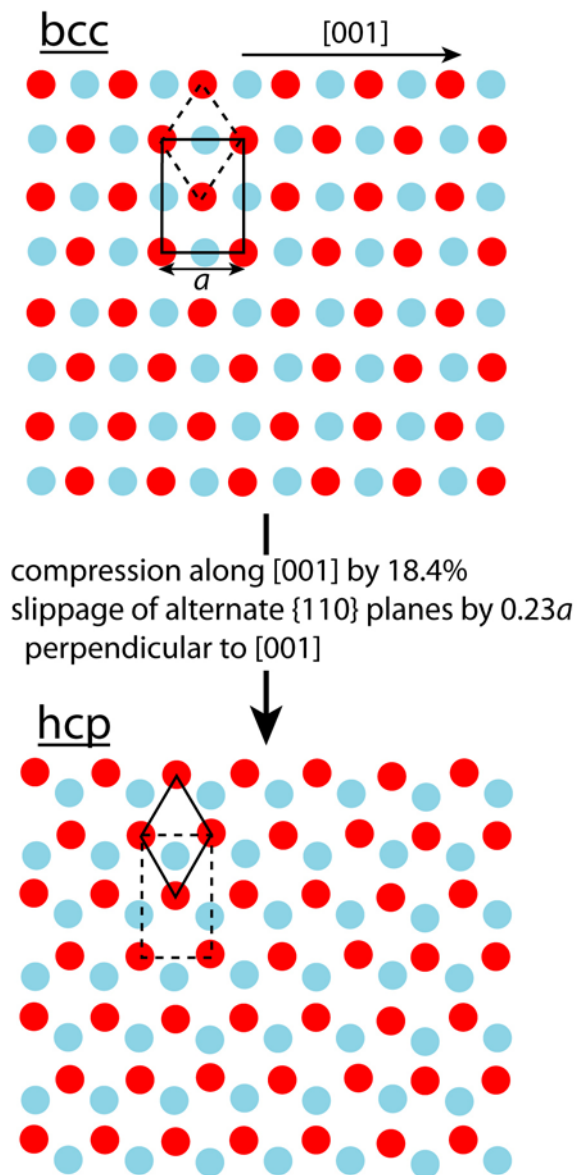


Figure S4. Schematic of the relationship between bcc and hcp packing (plan view) as described in the text. Rectangular and hexagonal unit cells are outlined in black to clarify the relation between the two structures. Note that the red sites are in the plane while the blue sites are $0.5 b$ lower in the b -direction.

Figure S3A contains GISAXS data for a thicker (300 nm) Brij 56 templated film synthesized under similar conditions as used for ultrathin films. The scattering pattern is indexed to the space group $Fmmm$ with unit cell parameters $a=82\text{\AA}$, $b=116\text{\AA}$, and $c=64\text{\AA}$, with the c axis perpendicular to the substrate. This is consistent with distorted bcc packing of micelles, aligned with $[110]$ perpendicular to the substrate, with $a = 82\text{\AA}$ and ca. 45% shrinkage along the z -axis. In-plane line width analysis shows a feature width limited by the resolution of the GISAXS instrumentation, indicating a lower bound for domain size of ca. 600 nm. Along the z -axis (through the thickness of the film), a lower limit of the packing domain size is estimated to be 125 nm. Also present in this GISAXS image is a diffuse halo; from the position of this halo along the y -axis ($q < q_{\text{bcc}}$), we posit that this diffuse scattering arises from defects in the bcc phase that indicate a nascent transformation to hcp.

For experimental convenience, the face-centered orthorhombic (fco) space group $Fmmm$ was used to simulate the bcc phase in both thin and thick nanoporous films²; this space group can describe $[110]$ -oriented bcc taking into account the uniaxial shrinkage perpendicular to the substrate seen in all EISA-derived films that results from drying stresses as well as silica condensation during film processing.

The unit cell for the $[001]$ -oriented hcp phase (space group $P6_3/mmc$) simulated in Figure 1A in main text is shown in Figure S3B, along with a schematic of the overall DNA translocation pathway through the film (C). Again, although the precise shape and connectivity of pores within the film is not known, we place a sphere at each lattice point of hcp packing to represent the likely positions of pores, and connect pores in C using the standard twelve-fold coordination between lattice points found in hcp packing.

Figure S4 illustrates the diffusionless transformation that relates bcc and hcp packing³. Although it is uncertain if the hcp phase seen in our ultrathin nanoporous films is derived from the bcc phase in this manner, the identical interplanar spacing between the two structures, as well as the relative orientation of the bcc and hcp lattice, are consistent with this mechanism. The hcp phase obtained by this transformation is not true hcp in the sense that $c/a \neq 1.57$; this distortion is further intensified by drying and condensation stresses during film assembly and template removal. Also, the micelles in this phase are not close packed. Nonetheless, we use the label ‘hcp’ as the pore arrangement and packing type (AB stacking of 2D hexagonal planes) are identical to true hcp.

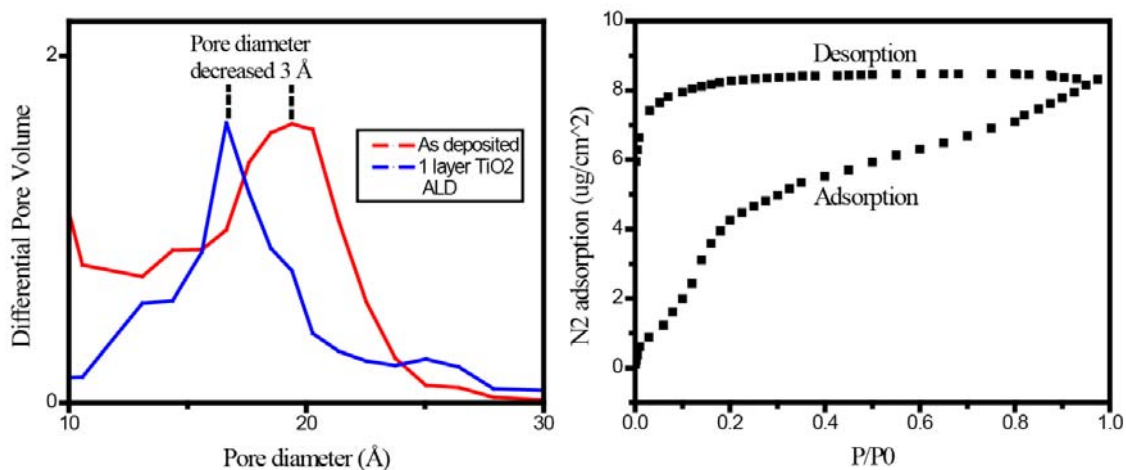


Figure S5. Pore size distribution of as deposited Brij 56 film and the same film after 1 layer of TiO₂ ALD calculated from adsorption branch of the N₂ adsorption data using a BJH model, showing ~ 3 Å pore size reduction after ALD (left); and the SAW acquired N₂ adsorption isotherm of Brij 56 film after 1 layer of TiO₂ ALD, showing extensive hysteresis on desorption branch, which is consistent with a constricted micropore network⁴ (right).

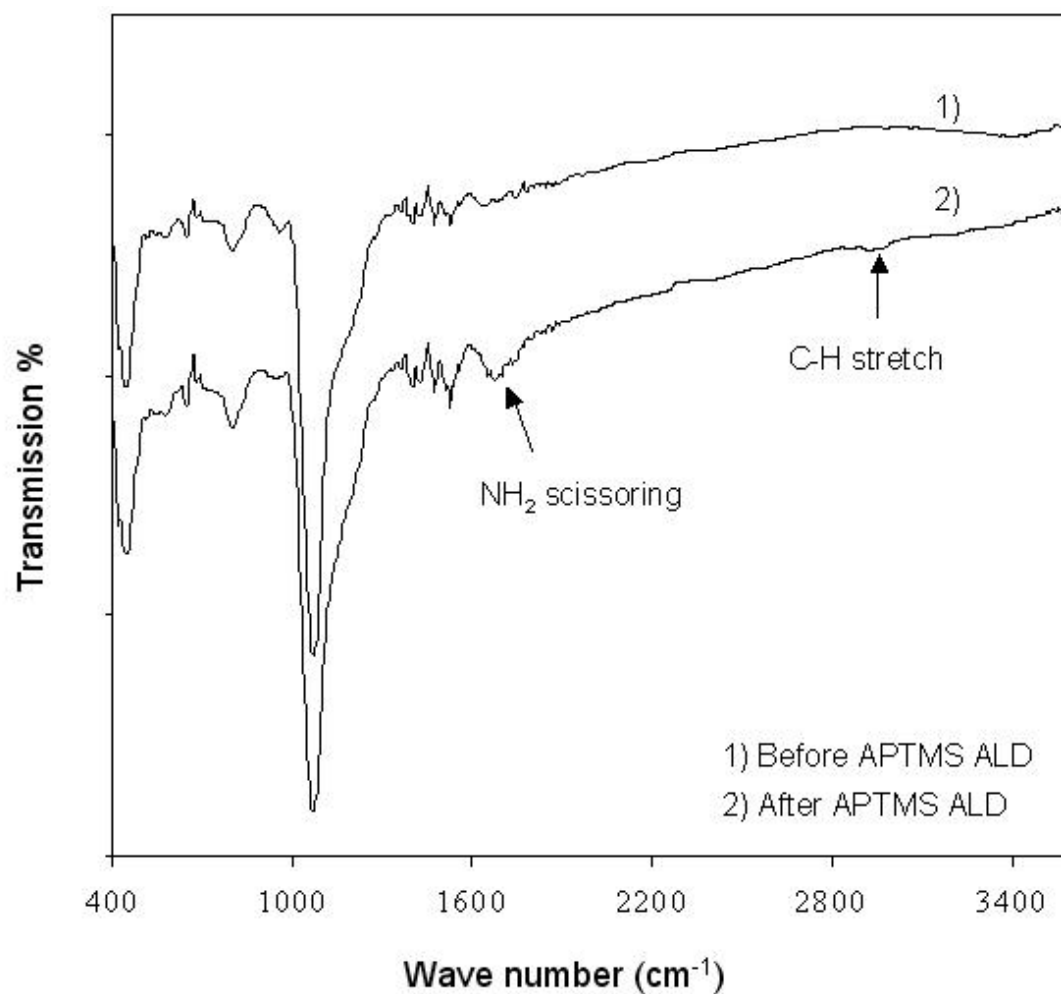


Figure S6. FTIR spectrum of mesoporous silica thin film before and after ALD of APTMS.

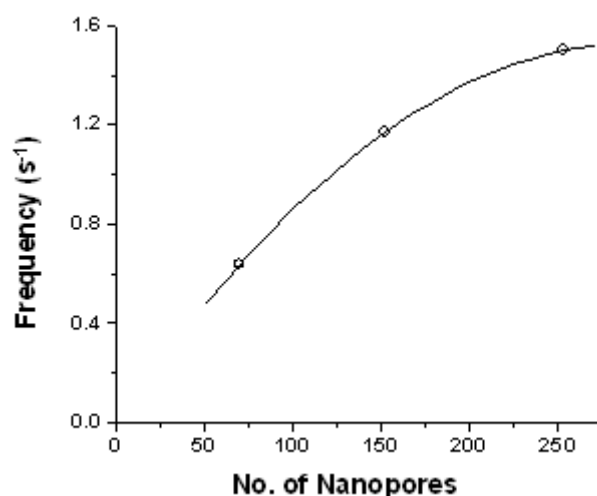


Figure S7. Current blockage frequency as a function of the number of nanopores confined by FIBed hole.

The nanopore array device is advantageous over the single solid-state nanopore for its possibility of fast and highly parallel readout of biological information. As we claimed in this article, the overall current blockage frequency is the sum of the dsDNA translocation events on all nanopores supported over the FIBed aperture. So current blockage frequency should increase with the number of nanopores above the aperture. Three parallel DNA translocation experiments were conducted on samples with FIBed apertures of three different sizes to study the frequency as a function of the number of nanopores. The selected aperture sizes are 40x56nm, 69x73nm and 86x95nm (the apertures are elliptical in shape so the area is determined from the long and short axes). The confined mesopore number after coating our thin film is calculated to be 70, 152 and 253 respectively. Figure S7 shows that the current blockage frequency increases with pore number, implying nanopore array device enhances the throughput of DNA translocation.

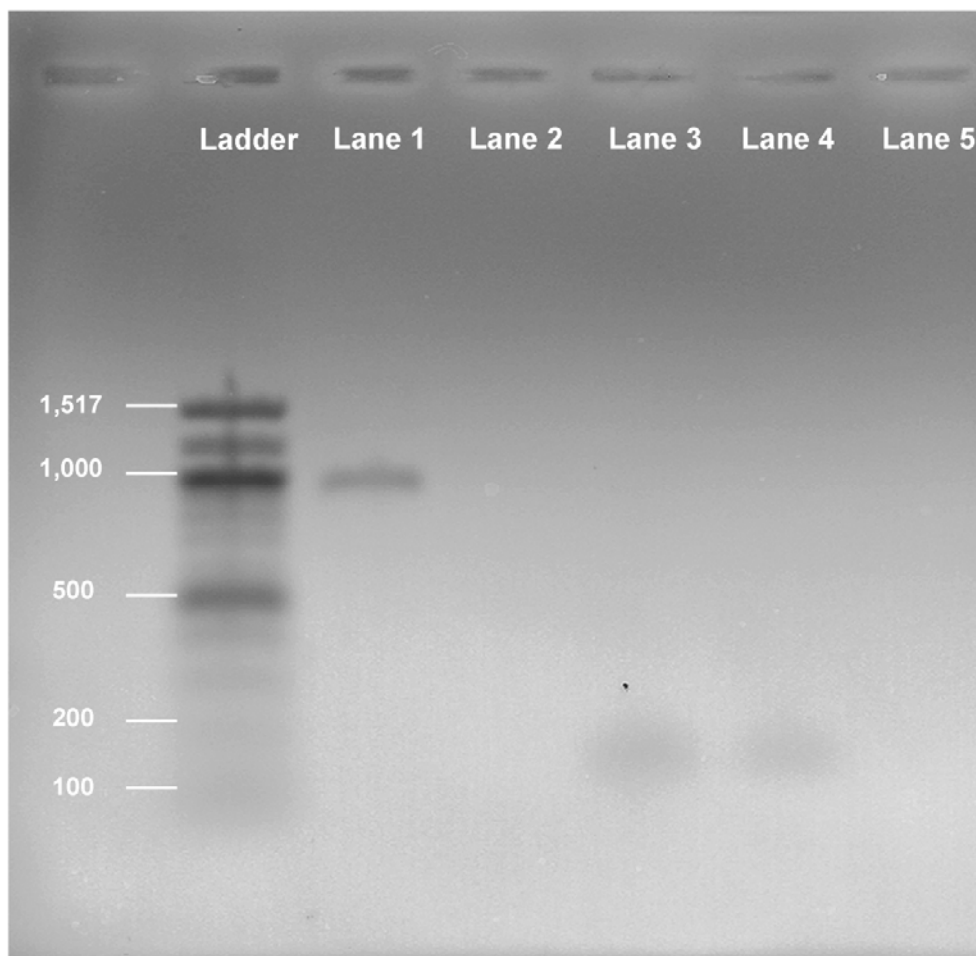


Figure S8. Lane 1: -trans solution after 950bp dsDNA in -cis was driven through membrane with 2.6-nm pores; Lane 2: -trans solution after 950bp dsDNA in -cis was driven toward membrane with 1.4-nm pores (after APTMS ALD treatment); Lane 3: -trans solution after 150b ssDNA in -cis was driven through membrane with 2.6-nm pores; Lane 4: -trans solution after 150b ssDNA in -cis was driven through membrane with 1.4-nm pores (after APTMS ALD treatment); Lane 5: -trans solution when 150b ssDNA was present in -cis side but no external voltage was applied.

To unambiguously demonstrate the selectivity of ssDNA over dsDNA after chemically modifying pore surface with aminopropyl trimethoxysilane (APTMS) with

ALD, we first applied membrane with no ALD treatment in our cell device and introduced specific dsDNA and ssDNA (in this case 950bp dsDNA amplified from pUC19 plasmid and 150b ssDNA with sequence described in Kasianowicz's paper⁵) individually in the -cis side of our cell. After applying external voltage to drive DNA moving toward -trans side for 1 hr, we collected solution from -trans side for each experiment. Then, we applied APTMS modified membrane in our cell device and repeated the above experiments with exactly the same procedure. To ensure the translocated polymers are not lost or washed away, the volume of total solution on the -trans side is carefully collected, especially for the area close to the membrane and electrode, a few rinsing steps are conducted and the rinsing solution is collected also. Before applying PCR amplification, we concentrated DNA using a cold ethanol precipitation protocol. After PCR amplification with well-designed high-specificity primers, we run electrophoresis and the results are shown as in Figure S8. Lanes 1, 3, 4 have single band after gel electrophoresis, representing the presence of one single length of DNA in each case after PCR (950bp for lane 1 and 150b for Lane 3 & 4). The results are consistent with DNA translocation results, showing dsDNA can only go through the pores before APTMS modification, while ssDNA can go through pores before and after APTMS modification.

We also conducted control experiments to make sure no contamination of DNA in DNA translocation experiments by collecting solution from -trans side after DNA was introduced in -cis side but no external voltage was applied. For both ssDNA and dsDNA, no band was observed after PCR amplification of -trans solution followed by gel electrophoresis.

Reference

1. Miyata, H. et al. Silica films with a single-crystalline mesoporous structure. *Nature Materials* 3, 651-656 (2004).
2. Urade, V. N. & Hillhouse, H. W. Synthesis of thermally stable highly ordered nanoporous tin oxide thin films with a 3D face-centered orthorhombic nanostructure. *Journal of Physical Chemistry B* 109, 10538-10541 (2005).
3. Kalantar, D. H. et al. Direct observation of the alpha-epsilon transition in shock-compressed iron via nanosecond x-ray diffraction. *Physical Review Letters* 95, 075502 (2005).
4. Gregg, S. J. & Sing, K. S. W. Adsorption, Surface Area and Porosity, 214 (1967).
5. Kasianowicz, J. J., Brandin, E., Branton, D. & Deamer, D. W. Characterization of individual polynucleotide molecules using a membrane channel. *Proceedings of the National Academy of Sciences of the United States of America* 93, 13770-13773 (1996).